Journal of New Materials for Electrochemical Systems 15, 89-95 (2012)

Graphene-Polythiophene Nanocomposite as Novel Supercapacitor Electrode Material

Farah Alvi[1], Punya A. Basnayaka[2], Manoj K. Ram[2,3], Humberto Gomez[2], Elias Stefanako[1,3], Yogi Goswami[3,4] and Ashok Kumar[2,3]

[1]Department of Electrical Engineering, University of South Florida, 4202 E Fowler Avenue, ENB 118, Tampa, FL, 33620
[2]Department of Mechanical Engineering, University of South Florida, 4202 E Fowler Avenue, ENB 118, Tampa, FL, 33620
[3]Nanotechnology Education and Research Center, University of South Florida, 4202 E Fowler Avenue, ENB 118, Tampa, FL, 33620
[4]Chemical & Biomedical Engineering Department, University of South Florida, 4202 E Fowler Avenue, ENB 118, Tampa, FL, 33620

Received: June 17, 2011, Accepted: November 16, 2011, Available online: December 22, 2011

Abstract: *The graphene (G)-polythiophene (PTh) nanocomposite was synthesized by a chemical oxidative polymerization technique and characterized using Field Emission Scanning Electron Microscopy (FESEM), High-Resolution Transmission Electron Microscopy (HRTEM), Raman Spectroscopy, Fourier transform Infrared spectroscopy (FTIR), X-ray-diffraction (XRD), Electrochemical Impedance spectroscopy(EIS) and cyclic voltammetry (CV) techniques. The electrochemical properties of G-PTh nanocomposite supercapacitor electrodes were investigated in different electrolytes solutions and a specific discharge capacitance of 154 F/g was estimated from different charge/discharge current cycles. Our proposed research is transformative as the G-conducting polymer based electrode material with unique and excellent properties, such as, high conductivity, wider tunable potential window, high stability of the electrode material in doped form, faster charge transfer rate, and short charging times, that allows the fabrication of high performance supercapacitors for practical applications.*

Keywords: graphene, polythiophene, nanocomposite, capacitance, supercapacitor, charging-discharging, conducting polymer, G-PTh, cyclic voltammetry.

1. INTRODUCTION

Supercapacitors are high efficiency energy storage devices representing an attractive alternative for portable electronics and automotive applications due to their high specific power and extended life [1-2]. The supercapacitor has been finding a number of applications because of its fast charge/discharge current in electric vehicles, backup sources for various electrical devices and uninterrupted power supplies, mobile/portable power/energy storage and handling including micro-autonomous robots, power hybrid vehicles, camera flash bulbs, pulsed laser distributed sensors, and other devices [3-4]. There is always a search for new materials to meet the requirements of high power density and long durability super capacitor devices for new demanding applications [5-8]. Recently, the importance of supercapacitors has been highlighted by the US department of energy (DOE) to be at the same level as rechargeable batteries. The nanoporous carbon, activated carbon, carbon nanotubes, metal oxides and conducting polymers (CPs) have been used in electrochemical supercapacitors as electrode materials [9-15]. Among them, CPs are widely considered as redox supercapacitors due to excellent electrochemical behaviors. CPs i.e., polypyrrole (PPy), polyaniline (PANI) and poly (3, 4-ethylenedioxythiophene) (PEDOT) with good electrical conductivity and large pseudo-capacitance have attracted wide interest as electrode materials for supercapacitor applications [16-18]. The nanoporous composite of Carbon Nanotubes (CNTs) and PPy, PANI–inorganic nanocomposites, graphite/PPy composites, p-doped poly (3-methylthiophene) (PMeT)/activated carbon systems, graphene-PANI and RuO_2/PPy have been fabricated [19-22].

The polythiophene (PTh) was first chemically synthesized in 1980 and since then it has been used in batteries and supercapacitor applications due to its high conductivity and stability [23-25].

*To whom correspondence should be addressed: Email:
Phone:

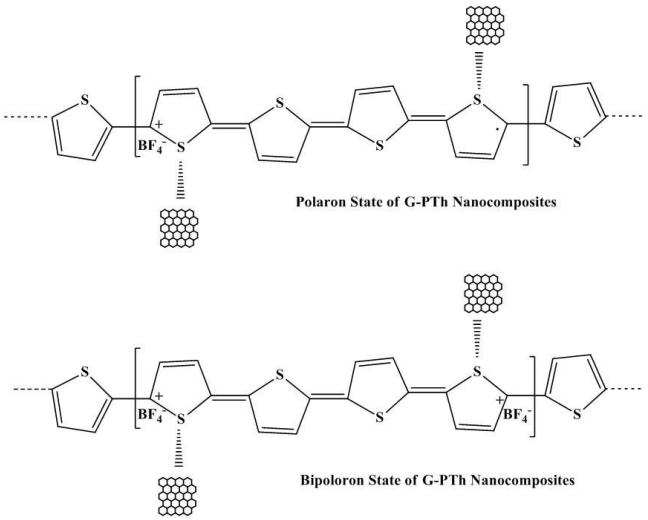

Figure 1. Schematic of G-PTh in two different forms in doped states

On the other hand, graphene, which is a two-dimensional honeycomb lattice structure of graphite, exhibits unusual and intriguing physical, chemical and mechanical properties, and recently, has been used in supercapacitors with and without the use of PPy and PANI CPs [26-27]. Graphene has been used as electrode material in supercapacitor applications in both aqueous (H_2SO_4, HCl, KOH) and nonaqueous electrolytic media ($LiClO_4$, $LiBF_6$, KCl etc.) [28-30].

Recently, we fabricated G-polyaniline and G-polyethylenedioxythiophene nanocomposite materials for supercapacitor applications [31-32]. A specific capacitance of 300 to 500 F/g at a current density of 0.1A/g was observed for G-PANI nanocomposite materials where 374 F/g was observed for G-PEDOT based supercapacitor electrodes. Our thrust of finding new materials has enabled us to develop the proper understanding of the structure and manufacturing properties of G–CPs nanocomposite films. The G–PTh nanocomposite was synthesized using a chemical oxidative polymerization technique and characterized using Field Emission Scanning Electron Microscopy (FESEM), TEM, FTIR, Raman spectrum and XRD. Supercapacitor properties such as cyclic voltammograms, charging/discharging, impedance and specific capacitance of G-PTh nanocomposite electrode materials in a supercapacitor have been studied at length.

2. EXPERIMENTAL

2.1. Synthesis of G-PTh nanocomposite material

The G-PTh nanocomposite was chemically synthesized by oxidative polymerization of thiophene using ammonium peroxydisulfate [$(NH_4)_2S_2O_8$)] and $FeCl_3$ under controlled conditions. Initially, the thiophene was dissolved in methanol. The polystyrene sulfonate Na salt (PSS) dissolved in HCl solution was set at 1PH for two hours. Next, the thiophene monomer in methanol was added to the PSS solution for two hours. The graphene nanoparticles purchased from Angstrom Materials (USA) was used without further purification. The thiophene to graphene ratio was kept at 1:1, and added to the PSS solution. The PSS solution was cooled down to -4°C in an ice bath before the drop wise addition of 0.05M Ammonium peroxydisulfate and 0.05M $FeCl_3$ oxidants. The final reaction was continued for 24 hours under constant stirring. The G-PTh nanocomposite recovered from the reaction vessel was filtered and washed thoroughly using deionized water, methanol (for the elimination of the low molecular weight polymer and oligomers). Further, the final precipitate was dried in a controlled-temperature oven at 100°C for 4 hours. Figure 1 shows the possible structure of the synthesized G-PTh nanocomposite polymer.

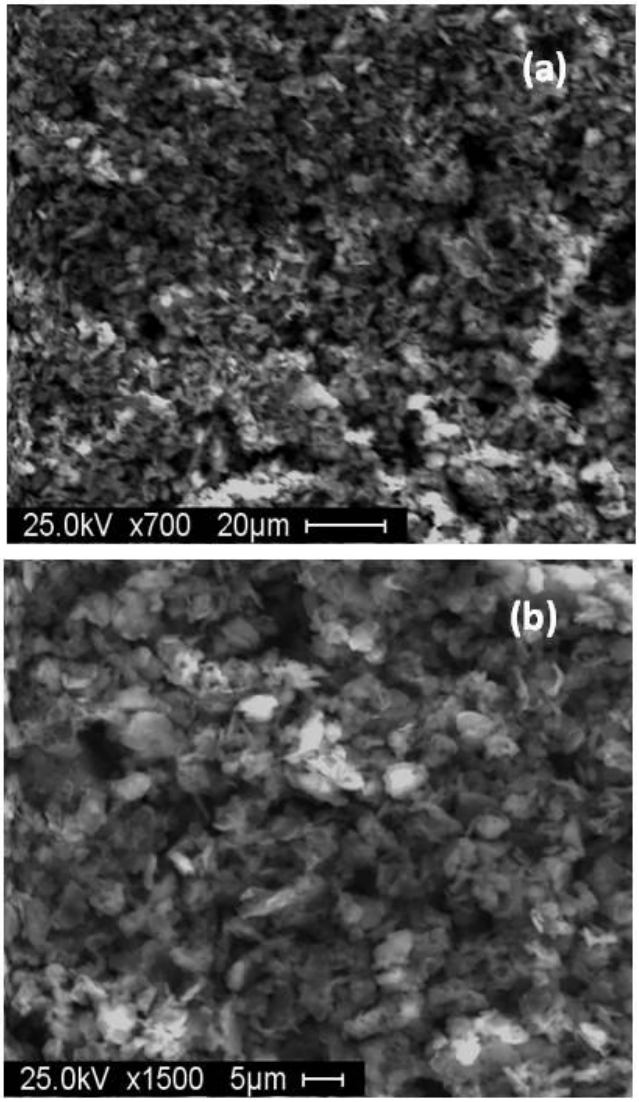

Figure 2. SEM images of G-PTh (a) size for 20 micron and (b) size for 5 micron

2.2. Optical Characterization of Films

The Raman studies on G-PTh were carried out in order to obtain information regarding the Raman Shift and absorption bands of inter or/and intra-gap states. The Raman spectrum of G-PTh was obtained by depositing the film on a n-type silicon substrate (100).

Figure 3. G-PTh TEM Pictures

2.3. Surface/Structure Characterization

The surface morphology and the size of the G-PTh films were then investigated by FESEM. The crystalline structure of the G-PTh nanocomposites was investigated using HRTEM and XRD techniques.

2.4. Electrode Preparation and Electrochemical setup

The synthesized G-PTh powder was mixed with nafion and the film was casted on a graphite substrate. The electrochemical measurements (cyclic voltammetry, charging/discharging and impedance) were measured in a cell containing the G-PTh nanocomposite as a working electrode, Pt as a counter electrode and Ag/AgCl as a reference electrode. The G-PTh film exhibited different conductivities on various substrates, with the best characteristics being obtained on Indium tin oxide (ITO) and graphite substrates. We have fabricated supercapacitors with G-PTh as electrode material in the electrolytic solutions 2M H_2SO_4, 2M HCl and 0.2 M $LiClO_4$.

3. RESULTS AND DISCUSSION

3.1. Scanning Electron Microscope (SEM) and Tunneling Electron Microscope Studies

Figure 2 shows the FESEM images taken with different magnifications. It is observed from the picture that a sponge-type structure is formed in G-PTh nanocomposite. The FESEM picture of graphene shows a flake type structure and large surface film area [31, 34]. In fact, the large surface area is also desirable for the supercapacitor application. This kind of porous electrode material is much promoted with electrolyte intercalation in return to good capacitance. Figure 3 shows a TEM picture of G-PTh, which reveals the graphitic laminar structure. The fibers in Fig. 3 are due to the PTh polymer on nanosheets in the backbone of graphene. A similar structure has been observed in our earlier studies [32-34].

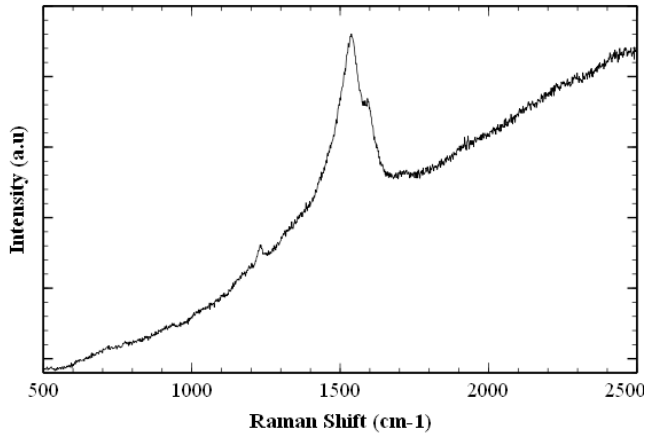

Figure 4. Raman Spectra for G-PTh nanocomposites

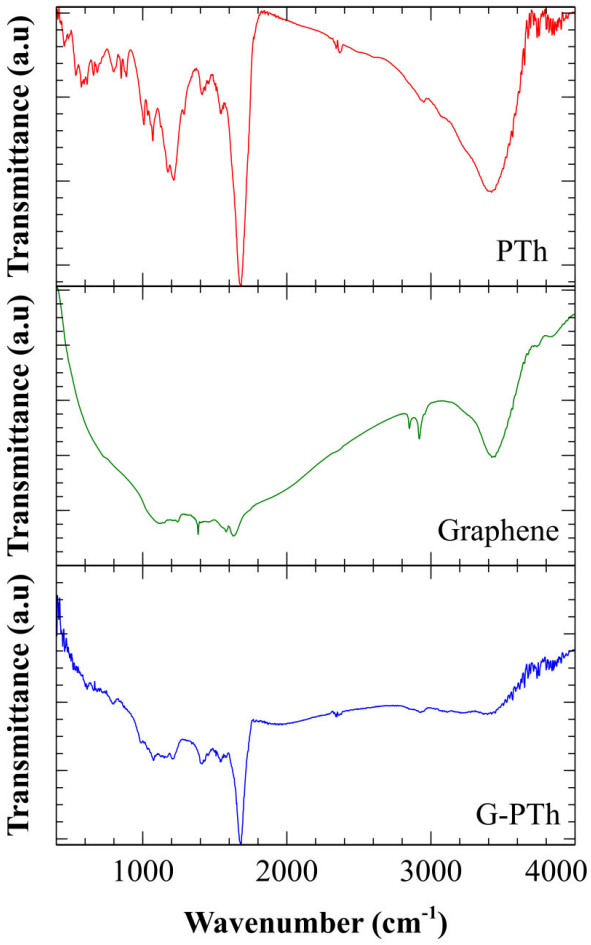

Figure 5. FTIR Spectra for PTh, G, G-PTh nanocomposites

3.2. Raman Studies

Figure 4 shows the Raman spectra of the G-PTh polymer on a silicon substrate. Raman bands can be observed at the peaks of feeble bands (736, 693), 1238, 1542, 1600, 1728 and 2421 cm^{-1}.

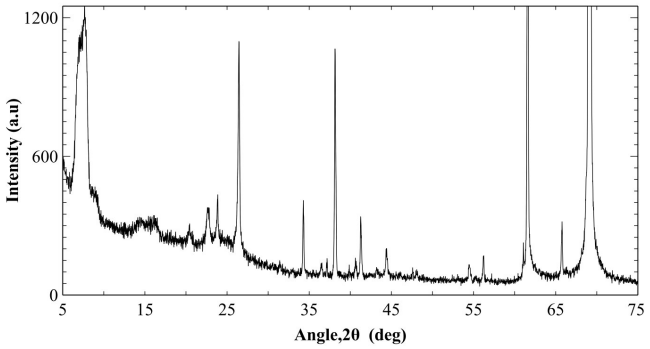

Figure 6. XRD of G-PTh nanocomposites

The typical G band due to graphene is located at 1600 cm^{-1}. The presence of the band at 1238 cm^{-1} is due to the C_{α}–$C_{\alpha'}$ stretching, the feeble bands at (736 cm^{-1} and 693 cm^{-1}) are the very characteristics C-S-C (rig deformation) of G-PTh [34].

3.3. FTIR

Figure 5 shows the FTIR spectra of the PTh, G, G-PTh nanocomposites measured using a KBr pellet. Figure 5 shows the FTIR spectra bands at 1434, 1649, 2902, 2966, 3447 cm^{-1} for graphene, bands at 570, 618, 708, 843, 891, 893, 1000, 1075, 1218, 1226, 1450, 1585, 1698, 2415, 1998, 3452, 3760, 3890 cm^{-1} for thiophene, and bands at 1458, 1708 $cm^{-1}$for G-PTh nanocomposite materials. The FTIR spectrum also shows the (C-H) stretching vibration band at 2923 cm^{-1}; (C=C) stretching band at 1458-1596 cm^{-1}; (C-H) in plane bending band at 1113 cm^{-1} and (C-S) bending band at 749 cm^{-1}. The C=C stretching vibration originating from the thiophene ring is also clearly observed at the band of 1585 cm^{-1}. The doping induced band at 1021 cm^{-1} is shown in the polymer chain with the counter ion balancing bands appearing at 1113, 1309 and 1458 cm^{-1} [35]. The characteristic bands of graphene for C- O and C–C are shifted to 1708 cm−1 and 1438 cm−1 due to the presence of G-PTh. The increased conjugation shifted to the absorption frequencies and resulted in the polymerization of G-PTh.

3.4. X-ray Diffraction

The XRD results of amorphous G-PTh are shown in Figure 6. The obtained XRD pattern shows the sharp and well-defined peaks, indicating the crystallinity of the synthesized material at 7.37, 8.25, 13.53, 15.11, 20.19, 22.55, 23.81, 26.43, 37.27, 38.13, 41.23, 61.49, 65.73 and 69.5 degrees. The obtained diffractogram (Fig. 6) exhibits not only the peaks of the PTh situated at the low angle 20.80°, which is typical characteristic of the polthiophene, but also exhibits the presence of graphene in it [36]. The average particle size of the G-PTh film was estimated based on the Scherer correlation for a particle diameter (d) with peak width. The average size of the particles calculated from the width of the diffraction peak, according to the Scherer equation, it is around 80 nm for the G-PTh nanocomposite.

3.5. Electrochemical Measurements

3.5.1. Cyclic Voltammetry Study

Cyclic voltammetry (CV) responses of the nafion mixed G-PTh film coated on graphite electrodes as a function of the scan rates of 10 mV/s (1), 20mV/s (2), 50mV/s (3) and 100 mV/s(4) are shown in figures 7 and 8.

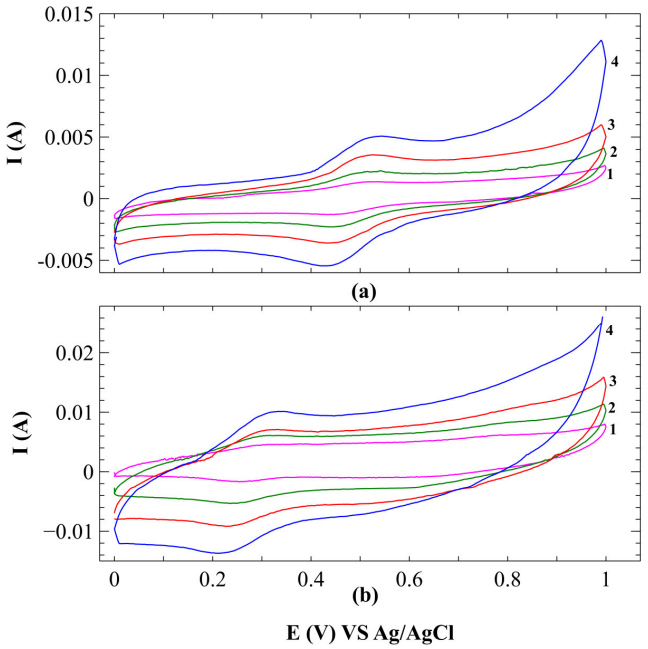

Figure 7. (a) Cyclic voltammetry of G–PTh in 2M HCl as function scan rates (1) 10, (2) 20 (3) 50 (4) 100 mV/sec; (b) Cyclic voltammetry of G–PTh in 2M H_2SO_4 as function scan rates, (2) 10, (3) 20 (4) 50 (5) 100 mV/sec

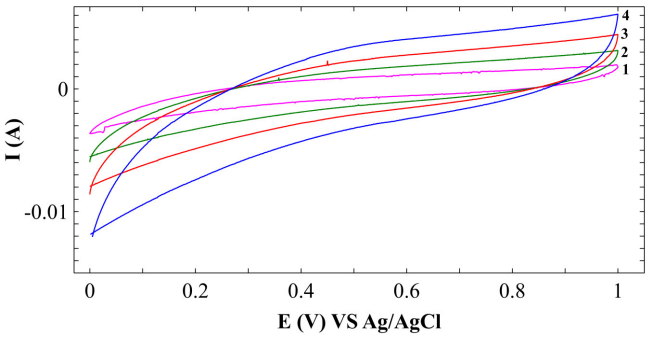

Figure 8. Cyclic voltammetry of G–PTh in 0.2 M $LiClO_4$ as function of scan rates, (2) 10, (3) 20 (4) 50 (5) 100 mV/sec

Figure 7(a, b) observes the CV measurements for a G-PTh based supercapacitor as a function of , 10, 20, 50, and 100mV/s scan rates in (2M HCl, 2M H_2SO_4). The CV studies reveal the pseudocapacitance in aqueous based HCl and H_2SO_4 electrolytes but lacks the pseudocapacitance in organic electrolyte contaning 0.2M $LiClO_4$. A distinct peak centered at 0.5 V corresponds to the oxidation of the G-PTh nanocomposite. The G-PTh nanocomposite also exhibits interesting electrochemical behavior showing the diffusion controlled mechanism where the conductivity is induced by a charge transferred doping mechanism. The doped and undoped

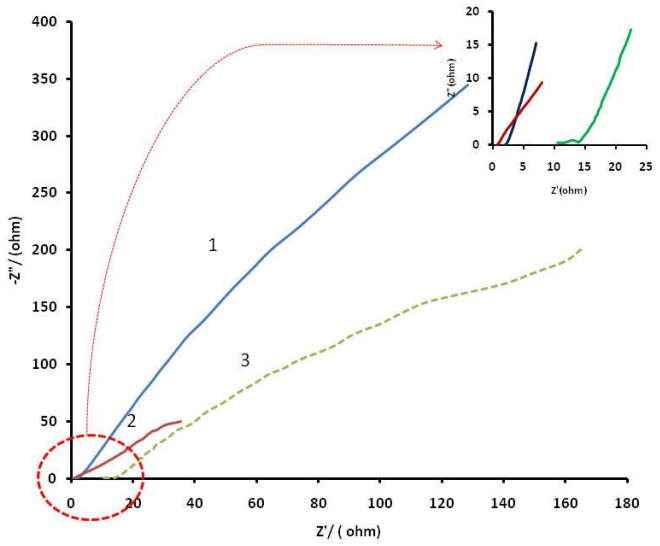

Figure 9. Nyquist plot of G–PTh at difffrent electrolytes (1) 2M HCl, (2) 2M H_2SO_4 and (3) 0.2 M $LiClO_4$

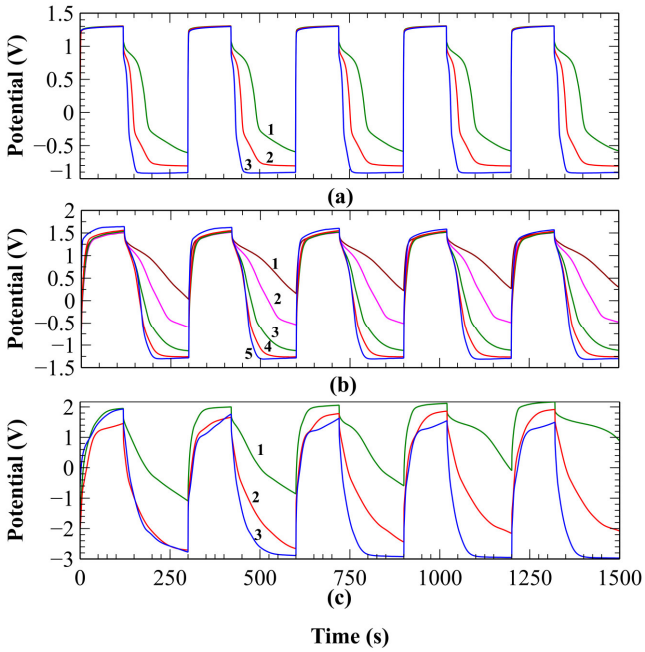

Figure 10. (a) Charging (20 mA) and discharging of G–PTh in 2M $LiClO_4$ as a function of discharge current (1) 5 mA (2) 10 (3) 20 mA; (b) Charging (40 mA) and discharging of G–PTh in 2M HCl as a function of discharge current (1) 5 mA (2) 10mA (3) 20 mA(4) 30mA and (5) 40 mA; (c) Charging (20 mA) and discharging of G–PTh in 2 M H_2SO_4 as a function of discharge current (1) 5 mA (2) 10 mA(3) 20 mA

states are responsible for the peaks, and the Faradaic transformation of the G-PTh initiates the redox behavior. It is also noted that the cathodic peaks (0.4 V) shift positively and the anodic peaks (0.65V) shift negatively as the voltage sweep rate changes from 10 mV/s to 100 mV/s.

Figure 8 also shows the CV profile of G–PTh films in 0.2M $LiClO_4$ as a function of scan rates (10, 20, 50, and 100mVs^{-1}). It reveals the reversible redox system with wide oxidation peaks at 0.53 V in a non-aqueous system. The specific capacitance was calculated for each scanning rate and it showed the increase in capacitance with a decrease in the scanning rate. This is basically due to the internal resistance of the capacitor.

The specific capacitance values of the supercapacitor from the respective cyclic voltammograms, shown in figures 7 and 8, have been calculated using equation (1),

$$C = i/s \qquad (1)$$

where s is the potential sweep rate and i is the specific current. The typical behavior of the capacitance as a function of scan rate can also be seen in Table 1 due to the charging and discharging mechanism of the capacitor. The specific capacitance value of the G-PTh nanocomposite is higher in H_2SO_4 than in HCl and $LiClO_4$.

Table 1.

Electrolyte	Current Density (A/g)	Specific capacitance (F/g)
0.2M $LiClO_4$	0.167	11.49
	0.333	27.9
	0.667	55.25
2M HCl	0.167	18.29
	0.333	32.00
	0.667	60.61
2M H_2SO_4	0.167	23.35
	0.333	30.49
	0.667	78.43
	1	116.20
	1.33	154.24

3.5.2. Impedance study

The Nyquist plot of G-PTh supercapacitor is shown in figure 9 for a frequency range from 100 kHz to 100 mHz. The Nyquist plot indicates a good capacitor-like behavior in the high frequency region. The internal resistances are found to be 0.7, 0.95 and 12.6 Ω in 2M H_2SO_4, 2M HCl and 0.2M $LiClO_4$, respectively. The Nyquist plot revealed that H_2SO_4 provides a high conductive medium. A small semicircle was observed in the high frequency region in the 0.2M $LiClO_4$ electrolyte. The small semicircle observed is due to the Faradic reactions. The charge transfer resistance estimated to be about 2Ω. However, there is no semicircle detected in impedance measurements of aqueous electrolytes in the high frequency range. This implies that both H_2SO_4 and HCl are more conductive than $LiClO_4$. The criterion for a G-PTh based supercapacitor to exhibit an ideal capacitor behavior is that the doping/dedoping rates are fast enough to provide a constant current during the redox reaction. This doping/dedoping process involves not only the charge (electrons or holes) transport but also the ionic transport. Here, the ionic transport rate determines the charge/discharge rate of the G-PTh, because it is slow compared to the charge transport.

3.5.3. Charging and discharging behaviour

The G-PTh supercapacitor electrochemical cell was tested for charge/discharge studies at a constant charging current density and

with different discharging current densities, as shown in figure 10 (a, b and c). The capacitor is charged and discharged from 1.2 to -1.2 V in 2M HCl, 1.5 to -1.5 V in 2M H_2SO_4 and 2.0 to -2.2 V in 0.2 M $LiClO_4$ electrolytic media. The discharge capacitance 'Cd' is evaluated from the discharge curves using the equation 2 [31].

$$C_d = \frac{I \times \Delta t}{\Delta V \times m} \quad (2)$$

Where I is the constant current, Δt is the time interval for a voltage change of V and m is the mass of the film coated over the graphite substrate. The estimated specific capacitance of a symmetric redox-type supercapacitor, from Figs 10 (a), (b), and (c), is shown in Table 1. It reveals that the maximum specific capacitance obtained in 2M H_2SO_4 shows a better system stability than in 2M HCl or 0.2 M $LiClO_4$. The columbic efficiency, η, was also calculated, using the equation η = charging time/discharging time)×100%, for three electrolytic media.

Charging and discharging of a G-PTh super capacitor in 0.2 M $LiClO_4$ at discharging currents of (1) 5mA, (2) 10 mA and (3) 20 mA is shown in figure 10 (a). At the 0.02 A/g current range, the maximum capacitance of the supercapacitors was calculated at 55 F/g, which is close to the value reported by cyclic voltammetry of 60 F/g for the $LiClO_4$ electrolyte.

Similarly figure 10(b) shows the charging and discharging characteristics of G-PTh in 2M HCl as a function of the discharging currents: (1) 5 mA, (2) 10 mA, (3) 20 mA, (4) 30mA and (5) 40mA. The charge/discharge profile of the supercapacitor at a constant current density of 40 mA/cm^2, labeled as curve 4, is similar to the 30 mA/cm^2 and remains between -1.50 to 1.5 V, for the first few cycles. From figure 10 (b), it is seen that the initial voltage drop during discharging is prominent and the voltage of the capacitor varies with time during both the charging and discharging processes for a number of different cycles. Figure 10 (c) demonstrates the specific capacitance in 2M H_2SO_4 at 20 mA/cm^2 estimated to be 154 F/g. The columbic efficiency of the supercapacitor calculated from the charge and discharge after 100 cycles was calculated to be in around 80% in 2M H_2SO_4, which has been found to be slightly different than in 2M HCl acidic media. However, in 2M H_2SO_4 at higher number of cycles the capacitance decreases slightly because of the decrease in redox activity of the supercapacitor. The charging and discharging has been found to be quite symmetrical in figure 10 (a, b, c) in spite of different electrolytes. The supercapacitor behavior of the G-PTh nanocomposite based supercapacitor has been understood using the electrochemical double layer capacitor (EDLC). The fast response of the charge accumulation occurs in an EDLC system with high reversibility. The ions and charge transport capabilities of electrolytes play a dominant role in improving the capacitance as well as the performance of the device.

4. CONCLUSIONS

A G-PTh nanocomposite material was synthesized by the oxidative polymerization technique and characterized using various physical and electrochemical techniques. The FTIR and Raman studies of G-PTh films have shown that graphene plays a dual role in improving the overall conductivity of a PTH system, by acting as a dopant and also forming nanocomposites with the PTh conducting polymer. The G-PTh structure dramatically improves the electrochemical performance in only PTh based supercapacitors. The G-PTh supercapacitor electrode provides a faster electrochemical reaction with an average capacity of 154 F/g. Further, the improvements in the electrochemical performance of supercapacitors can be obtained by optimizing the electrolytes, thickness of electrodes, cell design and the electrode material containing different ratios of thiophene to graphene in the nanocomposite structure. This study provides a fundamental understanding for high performance organic electronic devices based on PTh and graphene nanocomposite systems

5. ACKNOWLEDGEMENTS

This research was supported by the NSF grant # 0728100 and also partially supported by the NSF grant # 070734232.

REFERENCES

[1] E. Beaudrouet, A.L.G.L. Salle and D. Guyomard, Electrochimica Acta, 54, 1240 (2009).
[2] K.H. An, W.S. Kim, Y.Y.S. Park, J.M. Moon, D.J. Bae, S.C. Lim, Y.S. Lee and Y.H. Lee, Advanced Functional Materials, 11, 387 (2001).
[3] R.H. Baughman, A.A. Zakhidov and W.A.D. Heer, Science, 297, 787 (2002).
[4] R. Liu, S. Cho and S.B. Lee, Nanotechnology, 19, 1 (2008).
[5] M.W. Mehrens, J. Schenk, P.M. Wilde, E. Abdelmula, P. Axmann, J. Garche, Journal of Power Sources, 105, 182 (2002).
[6] F.E. Amitha, A.L.M. Reddy and S. Ramaprabhu, Journal of Nanoparticles, 11, 725 (2009).
[7] R.E. Metallurgiche, U.C.D. Istituti, S. Chimiche, Solid State Ionics, 148, 493 (2002).
[8] A.I. Najafabadi, S. Yasuda, K. Kobashi, T. Yamada, D.N. Futaba, H. Hatori, M. Yumura, S. Iijima, and K. Hata, Advanced Energy Materials, 22, 235 (2010).
[9] J.P. Ferraris, M.M. Eissa, I.D. Brotherston and D.C. Loveday, Chemistry of Materials, 10, 3528 (1998).
[10]B.E. Conway and W.G. Pell, Journal of Solid State Electrochemistry,7, 637 (2003).
[11]A. Janes, H. Kurig and E. Lust, Carbon, 45, 1226 (2007).
[12]E. Frackowiak and F. Beguin, Carbon, 39, 937 (2001).
[13]H. Pan, J. Li and Y.P. Feng, Nanoscale Research Letters, 5, 654 (2010).
[14]A.L.M. Reddy and S. Ramaprabhu, Journal of Physical Chemistry, 11, 7727 (2007)
[15]C.C. Hu, K.H. Chang, M.C. Lin and Y.T. Wu, Nano Letters, 6, 2690 (2006).
[16]B. Muthulakshmi, D. Kalpana, S. Pitchumani and N.G. Renganathan, Journal of Power Sources, 158, 1533 (2006).
[17]V. Gupta and N. Miura, Materials Letters, 60, 1466 (2006).
[18]K.S. Ryu, Y.G. Lee, Y.S. Hong, Y.J. Park, X. Wu, K.M. Kim, M.G. Kang, N.G. Park, S.H. Chang, Electrochimica Acta, 50, 843 (2004).
[19]M. Hughes, G.Z. Chen, M.S.P. Shaffer, D.J. Fray and A.H. Windle, Chemistry of Materials, 14, 1610 (2002).
[20]C. Zhou, S. Kumar, C.D. Doyle and J.M. Tour, Chemistry of

Materials, 17, 1997 (2005).
[21]H. Wang, Q. Hao, X. Yang, L. Lu and X. Wang, Nanoscale, 2, 2164 (2010).
[22]B.O. Park, C.D. Lokhande, H.S. Park, K.D. Junga O.S. Joo, Journal of Power Sources, 134, 148 (2004).
[23]A.D. Marani, A.A. Entezami, Iranian Journal of Polymer Science and Technology, 3, 2 (1994).
[24]A. Laforgue, P. Simon, C. Sarrazin, J.F. Fauvarque, Journal of Power Sources, 80, 142 (1999).
[25]S.R.P. Gnanakan, N. Murugananthem and A. Subramania, Polymer Advanced Technologies, 2009.
[26]S.R.C. Vivekchand, C.S. Rout, K.S. Subrahmanyam, A. Govindaraj and C.N.R. Rao, Journal of Chemical Scicience, 120, 9 (2008).
[28]Y. Wang, Z. Shi, Y. Huang, Y. Ma, C. Wang, M. Chen and Y. Chen, Jornal of Physical Chemistry C, 113, 13103 (2009).
[29]M.D. Stoller, S. Park, Y. Zhu, J. An and R.S. Ruoff, Nano Letters, 8, 3498 (2008).
[30]C. Liu, Z. Yu, D. Neff, A. Zhamu, and B.Z. Jang, Nano Letters, 10, 4863 (2010).
[31]H. Gomez, M.K. Ram, F. Alvi, P. Villalba, L. Stefanakos, A. Kumar, Journal of Power Sources, 196, 4102 (2011).
[32]F. Alvi, M. K. Ram, Punya A. Basnayaka, E. Stefanakos Y.Goswami, A. Kumar, Electrochimica Acta, 56, 9406 (2011).
[33]S. Stankovich, D.A. Dikin, G.H.B. Dommett, K.M. Kohlhaas, E.J. Zimney, E.A. Stach, D. Piner, S.T. Nguyen and R.S. Ruoff, Nature letters, 442, 282 (2006).
[34]G. Shi, J. Xu and M. Fu, Journal of Physical Cheistry B, 106, 288 (2001).
[35]H.S. Nalwa, "Handbook of advanced electronic and photonic materials and devices," vol. 2, 2001.
[36]Z.Q. Li, C.J. Lu, Z.P. Xia, Y. Zhou, Z. Luo, Carbon, 45, 1686 (2007).